ABSTRACT

BABU, GODFREY MATHIAS LEMUNGE. Computation of Complex Band Structures of Phononic Crystals and Metamaterials through Padé Interpolation (Under the direction of Dr. Murthy Guddati).

Complicated elastic and acoustic wave propagation in phononic crystals and metamaterials are characterized through band structures. Specifically, complex band structures provide insight not only into propagation but also into evanescence of wave modes, but requires significant computational effort, especially for realistic three-dimensional unit cells.

The computational cost can be reduced with the help of modal reduction technique, which is based on reducing the number of degrees of freedom through projection of a reduced space spanned by appropriately chosen modes. While this approach reduces the computational cost, it still requires large number of basis vectors making the computation expensive. In this thesis, we introduce an idea that facilitates the computation only at a sparse set of frequencies, leading to practical computation of complex band structures for complicated unit cells.

The basic ingredients of the proposed methodology are to compute the wave numbers for sparse set of frequencies and interpolate the band structure on to a dense frequency grid. We utilize piecewise Padé interpolation for this purpose, which is known to be superior to more common polynomial interpolation. We develop strategies to (a) automatically identify Padé intervals based on computing resonant frequencies at the center and the edges of the irreducible Brillouin zone, and (b) ad hoc but automatic selection of Padé interpolation points in these intervals. The effectiveness of the proposed approach is illustrated through computing the complex band structures for 1D and 2D phononic crystals as well as metamaterials. We consider both damped

and undamped structures. For all the cases, the proposed approach appears effective, clearly capturing even the complicated branches of the complex band structures.

Computation of Complex Band Structures of Phononic Crystals and Metamaterials through Padé Interpolation

by
Godfrey Mathias Lemunge Babu

A thesis submitted to the Graduate Faculty of
North Carolina State University
in partial fulfillment of the
requirements for the degree of
Master of Science

Civil Engineering

Raleigh, North Carolina
2020

APPROVED BY:

Dr. Murthy Guddati
Committee Chair

Dr. Gracious Ngaile

Dr. Gnanamanikam Mahintharkumar

DEDICATION

To my lovely wife, Alease and my darling princess, Montgomerie.
You both make my world go around

BIOGRAPHY

Godfrey Babu was born and raised in the United Republic of Tanzania. He attended secondary school at a minor catholic seminary in Mara region, where he became fascinated with Newtonian mechanics. In 2007, he was admitted to the University of Dar es Salaam to pursue Bachelor of Science in civil and structural engineering, for which he graduated a class of 2011 with honors.

Upon completion of the first degree, he took positions in several companies and served as a structural engineer for four years before he immigrated to the United States by the end of 2015. He later enrolled for the Master of Science in computational mechanics in the following year to study under Professor Murthy Guddati at North Carolina State University.

Babu is married to Alease, they welcomed their daughter Montgomerie in 2016.

ACKNOWLEDGMENTS

The completion of this body of work was both a challenging, yet rewarding task that could not have been completed without contributions from the following: First and foremost, I would like to give honor to God, the almighty who gave me the strength to endure.

My family that supported and encouraged me to continue to move forward until the end. My advisor, Professor Murthy Guddati who motivated me even before I began my graduate studies and then granted me the to work together on the completion of this project.

Thank you to all the committee members: Professor Gracious Ngaile and Professor Gnanamanikam Mahintharkumar and others who have contributed along the way but are not necessarily named, my sincere gratitude and appreciation.

TABLE OF CONTENTS

LIST OF TABLES

LIST OF FIGURES

1. Introduction

1.1 Background and Motivation

The ability to manipulate and control acoustic and elastic waves breathed a new excitement in the wave propagation community with the discovery of phononic crystals and phononic-metamaterials [1]-[2]. These are artificial media with geometric configurations consisting of periodic arrangement of scatterers inside host (matrix) with different material properties to form a *more than one* material phase topology in 1D, 2D or 3D layouts. The attractive dynamic property of a *phononic crystal*, with sufficiently large contrast between integral components' mechanical characteristics, is the possibility of the presence of a frequency range from which waves are prohibited from propagating due to *Bragg scattering* phenomenon [3]. This band of frequency, which is subject to spatial modulation of the phononic crystal is referred to as *Bragg bandgap* [4]. In contrast, phononic *metamaterials* have gained much attention since their inception in the early 2000's due to their fascinating ability to exhibit bandgaps at subwavelength regime. This is often due to the presence of internal resonator engineered inside a phononic crystal [5].

Understanding the wave propagation in phononic crystals and metamaterials requires computation of *Band structures* or *Complex band structures*, which provide the dispersion relations linking frequency(ω) and wavenumber (k). The latter, i.e. complex band structures, are more general representation of dispersion relations which includes both propagating as well as evanescent (non-propagating) modes [6]. Unlike real band structures, complex band structures contain imaginary part of wave number k and plotted against real frequencies ω to reveal the edge modes. While the standard $\omega(k)$ formulation for computation of band structure is relatively efficient, the efficiency comes at the cost of not characterizing non-propagating *waves* [7, 8]. Dispersion curves, when viewed in complex plane, are no longer discontinuous at the boundaries [9]. Instead, evanescent waves provide information of exponential decaying ability of the edge modes and have applications, e.g. for high resolution imaging at near field zones [8].

An early 1D finite element formulation of $k(\omega)$ by Bavencoffe et al. [6] and latter extension to higher dimension by Vares, et al. [8] used Wave Finite Element Method (WFEM), whereas periodic boundary conditions for a unit cell was enforced through Floquet propagators in a transfer matrix. While WFEM was successful for 1D complex band structure modelling, computation for higher dimension systems were only limited to propagation in high symmetry direction since intermediate propagation directions resulted into irrational number for the order of eigenvalue problem. A variant of general $k(\omega)$ approach in finite element contexts that allows for damping and propagation from all polarizations presented in e.g., [10] is adapted in this study.

Complex-band computation by $k(\omega)$ approaches are computationally demanding due to the higher order eigenvalue problem and associated *frequency sweeping* cost. A mode synthesis reduction-type technique for complex band structures [11] is built on WFEM and address some reduction in system matrix size leading to cost savings. However, for three dimensional systems, the cost is still significant and further reduction in computational cost is desired.

In this thesis, we focus on reducing the number of frequencies for which complex band computation is performed, based on *Padé interpolation* approach. Computational cost reduction by Padé technique has been used in structural dynamics and other areas [12]. The effectivenes is determined based on the choice of Padé interpolation points and Padé intervals which are problem specific. We provide a systematic approach to compute complex band structure for sparse set of frequencies, and interpolate onto dense frequency grid. Essentially, given the periodic cell, we propose an algorithm to systematically obtain the Padé interpolation points and intervals automatically to reuslt in accurate complex band structure on a dense grid frequencies.

The outline of this thesis is as follows: in Chapter 2, we present the Bloch-Floquet formulation for computation of complex band structures. In Chapter 3, we expound on the proposed reduction computational cost by piecewise Padé interpolation. Several numerical examples are shown in Chapter 4, clearly illustrating the effectiveness of the proposed technique. We conclude the thesis with some closing remarks in Chapter 5.

2. Wave Propagation in Periodic Structures

2.1 Problem Statement

Solution for a travelling wave in periodic media, often referred to as *Bloch Function,* was early on realized from *Bloch theorem* postulated by Felix Bloch [13] to solve the Schrödinger equation. The formalism is equally applicable to general periodic systems including phononic crystals and metamaterials. Due to the underlying translational symmetry of the media, the Bloch function, denoted as $\boldsymbol{u}(\boldsymbol{x})$, *which is not periodic itself,* takes the form of a plane-wave modulated by a periodic function:

$$\boldsymbol{u}(\boldsymbol{x}) = \widetilde{\boldsymbol{u}}(\boldsymbol{x})e^{i\boldsymbol{k}.\boldsymbol{x}}, \tag{2.1}$$

where $\widetilde{\boldsymbol{u}}(\boldsymbol{x})$ is a periodic function, i.e.,

$$\widetilde{\boldsymbol{u}}(\boldsymbol{x}) = \widetilde{\boldsymbol{u}}(\boldsymbol{x}+\boldsymbol{p}), \tag{2.2}$$

and $\boldsymbol{x} = \{x_1,\ x_2,\ x_3\} \in \mathbb{R}^3$ is the position vector, $\boldsymbol{k} = \{k_1,\ k_2,\ k_3\} \in \mathbb{C}^3$ is the wavenumber vector, and $\boldsymbol{p}$ is the translational vector associated with periodicity of the media.

The governing differential equation for a continuous system to describe vibration field is given by the elastodynamic equation,

$$-\mathscr{L}^{\mathrm{T}}(\boldsymbol{E}\mathscr{L}\boldsymbol{u}) + \rho\,\ddot{\boldsymbol{u}} = \boldsymbol{0}, \tag{2.3}$$

where $\mathscr{L}$ is (generalized) gradient operator, $\boldsymbol{E}$ is elasticity matrix and ρ is material density. For phononic crystals and metamaterials , Bloch function in Eq. (2.1) must satisfy Eq. (2.3), which translates to finding the periodic function $\widetilde{\boldsymbol{u}}(\boldsymbol{x})$ and the corresponding wavenumber vector $\boldsymbol{k}$.

2.2 Complex Band Structures

The propagation characteristics of periodic media including features such as bandgaps, are understood through the dispersion relation, which relates the temporal frequency to the wavenumber. The traditional approach computes the (real-valued) frequency given the (real-valued) wavenumber, which results the characterization of bandgaps; this is referred to as the real band structure. An alternative approach, where the (complex-valued) wave number is computed as a function of (real-valued) frequency, is referred to as complex band structure. This representation of dispersion relations not only captures the band gaps, but also quantifies the level of evanescence within these bandgaps (through imaginary part of the wave number). In this thesis, we focus on the computation of complex band structures.

Propagative Bloch waves in space ($\boldsymbol{x}$) and harmonic in time (t) follows from Eq. (2.1) and Eq. (2.2) in that,

$$\boldsymbol{u}(\boldsymbol{x},t) = \widetilde{\boldsymbol{u}}(\boldsymbol{x})e^{i(\boldsymbol{k}.\boldsymbol{x}-\omega t)} \,. \tag{2.4}$$

A resulting *Bloch-elastodynamic* strong form is obtained by substituting Eq. (2.4) into Eq. (2.3),

$$-\,\mathscr{L}^{\mathrm{T}}\left(\,\boldsymbol{E}\,(\,\mathscr{L}\,\widetilde{\boldsymbol{u}} + \boldsymbol{L}_{\boldsymbol{k}}\,\widetilde{\boldsymbol{u}}\,)\,e^{i(\boldsymbol{k}.\boldsymbol{x}-\omega t)}\,\right) - \,\omega^2\rho\,\widetilde{\boldsymbol{u}}\,e^{i(\boldsymbol{k}.\boldsymbol{x}-\omega t)} = \boldsymbol{0}, \tag{2.5}$$

where,

$$\boldsymbol{L}_{\boldsymbol{k}} = i\kappa\,\boldsymbol{L}_{\theta}, \tag{2.6}$$

where, $\kappa = |\boldsymbol{k}|$ and $\boldsymbol{L}_{\theta}$ is a unit vector representing propagation direction e.g., for 2D plane strain elasticity conditions, $\boldsymbol{L}_{\theta} = \begin{bmatrix} \cos\theta & 0 \\ 0 & \sin\theta \\ \sin\theta & \cos\theta \end{bmatrix}$ for any propagation direction θ.

Further simplification of Eq. (2.5) results into,

$$-\mathscr{L}^{\mathrm{T}}\boldsymbol{E}\,(\mathscr{L}\,\widetilde{\boldsymbol{u}}+\boldsymbol{L_k}\,\widetilde{\boldsymbol{u}})\,-\boldsymbol{L_k}^{\mathbf{T}}\,\boldsymbol{E}\,(\mathscr{L}\,\widetilde{\boldsymbol{u}}+\boldsymbol{L_k}\,\widetilde{\boldsymbol{u}})-\,\omega^2\rho\,\widetilde{\boldsymbol{u}}=\mathbf{0}. \qquad (2.7)$$

The corresponding weak form is obtained after multiplying Eq. (2.7) by an arbitrary test function $\boldsymbol{\delta\widetilde{u}}$, integrating over the unit cell Ω and applying integration by parts,

$$\int_{\Omega}(\mathscr{L}\boldsymbol{\delta\widetilde{u}})^{\boldsymbol{T}}\,\boldsymbol{E}\,(\mathscr{L}\,\widetilde{\boldsymbol{u}}+\boldsymbol{L_k}\,\widetilde{\boldsymbol{u}})\,d\Omega-\int_{\Omega}\boldsymbol{\delta\widetilde{u}^{T}}\,\boldsymbol{L_k}^{\boldsymbol{T}}\boldsymbol{E}\,(\mathscr{L}\,\widetilde{\boldsymbol{u}}+\boldsymbol{L_k}\,\widetilde{\boldsymbol{u}})\,d\Omega$$

$$-\int_{\Omega}\boldsymbol{\delta\widetilde{u}^{T}}\omega^2\rho\,\widetilde{\boldsymbol{u}}\;\,d\Omega=\mathbf{0}. \qquad (2.8)$$

Finite Element formulation is obtained by employing Bubnov-Galerkin discretization, i.e.,

$$\begin{cases}\widetilde{\boldsymbol{u}}(\boldsymbol{x})\approx\boldsymbol{N}(\boldsymbol{x})\,\boldsymbol{d},\\ \boldsymbol{\delta\widetilde{u}}(\boldsymbol{x})\approx\boldsymbol{N}(\boldsymbol{x})\,\boldsymbol{\delta d},\end{cases}$$

where, $\boldsymbol{N}$ is interpolation functions space, $\boldsymbol{d}$ is nodal displacement and $\boldsymbol{\delta d}$ is test function’s nodal displacement. Substituting the above expressions in Eq. (2.8) results in,

$$\left[\int_{\Omega}(\mathscr{L}\,\boldsymbol{N})^{\boldsymbol{T}}\boldsymbol{E}\,(\mathscr{L}\,\boldsymbol{N}+\boldsymbol{L_k}\boldsymbol{N})\,d\Omega-\int_{\Omega}\boldsymbol{N^T}\,\boldsymbol{L_k}^{\boldsymbol{T}}\boldsymbol{E}(\mathscr{L}\,\boldsymbol{N}+\boldsymbol{L_k}\boldsymbol{N})\,d\Omega\right.$$

$$\left.-\,\omega^2\int_{\Omega}\boldsymbol{N^T}\rho\boldsymbol{N}\;\,d\Omega\right]\boldsymbol{d}=\mathbf{0}. \qquad (2.9)$$

Noting that $\boldsymbol{k}$ has unknown magnitude κ and fixed propagation direction θ, and substituting Eq. (2.6) into Eq. (2.9) results in,

$$\left[\int_{\Omega}\boldsymbol{\mathcal{B}^T}\,\boldsymbol{E}\,\boldsymbol{\mathcal{B}}\;\,d\Omega+i\kappa\int_{\Omega}\boldsymbol{\mathcal{B}^T}\,\boldsymbol{E}\,\boldsymbol{L}_{\theta}\boldsymbol{N}\,d\Omega-i\kappa\int_{\Omega}\boldsymbol{N^T}\;\boldsymbol{L}_{\theta}{}^{T}\boldsymbol{E}\,\boldsymbol{\mathcal{B}}\,d\Omega\right.$$

$$-\kappa^2 \int_\Omega \boldsymbol{N^T} \boldsymbol{L}_\theta{}^T \boldsymbol{E}\, \boldsymbol{L}_\theta \boldsymbol{N}\ d\Omega - \ \omega^2 \int_\Omega \boldsymbol{N^T} \rho \boldsymbol{N}\ d\Omega \Bigg] \ \boldsymbol{d} = \boldsymbol{0}\,, \tag{2.10}$$

where $\boldsymbol{\mathcal{B}}$ is the strain-displacement matrix,

$$\boldsymbol{\mathcal{B}} = \mathscr{L}\ \boldsymbol{N}. \tag{2.11}$$

Eq. (2.10) can be represented as,

$$[(-\omega^2 \boldsymbol{\mathcal{M}} + \boldsymbol{\mathcal{K}}) + i\kappa\, \mathbf{H}(\theta) - (i\kappa)^2 \boldsymbol{A}(\theta)]_{\Omega_n} \boldsymbol{d} = \boldsymbol{0}, \tag{2.12}$$

where,

$$\boldsymbol{\mathcal{K}} = \int_\Omega \boldsymbol{\mathcal{B}^T}\, \boldsymbol{E}\, \boldsymbol{\mathcal{B}}\, d\Omega\ ;\ \mathbf{H} = \int_\Omega (\boldsymbol{\mathcal{B}^T}\, \boldsymbol{E}\, \boldsymbol{L}_\theta \boldsymbol{N}\ - \boldsymbol{N^T}\ \boldsymbol{L}_\theta{}^T \boldsymbol{E}\, \boldsymbol{\mathcal{B}})\, d\Omega\, ; \boldsymbol{A} = \int_\Omega \boldsymbol{N^T} \boldsymbol{L}_\theta{}^{\boldsymbol{T}} \boldsymbol{E} \boldsymbol{L}_\theta \boldsymbol{N}\ d\Omega,$$

and

$$\boldsymbol{\mathcal{M}} = \int_\Omega \boldsymbol{N^T} \rho \boldsymbol{N}\ d\Omega\, .$$

Eq. (2.12) is the $\boldsymbol{k}(\omega)$ formulation. Periodic boundary conditions on a unit cell are conveniently applied on system matrices $\boldsymbol{\mathcal{K}}$, $\mathbf{H}$, $\boldsymbol{A}$ and $\boldsymbol{\mathcal{M}}$. Complex band structure can therefore be computed by fine sweeping ω in Eq. (2.12) for any propagation direction θ.

2.3 Model Problem

Consider a 1D undamped bi-material phononic crystal (a continuous bar); the periodic cell is shown in Figure 2.1(a), where periodic boundary conditions are applied. Contrast between material properties is made relatively high to enhance the band structure. Solving Eq. (2.12) and fine-sweeping through temporal frequencies $\omega,$ result in the complex band structure shown in Figure 2.1(b), which is plotted for both the real part of $\boldsymbol{k}$ (propagating branches) and the imaginary of $\boldsymbol{k}$ (evanescent modes). Real band structure is shown in Figure 2.1(d), which shows Bragg bandgaps at certain frequency ranges. The imaginary part of the dispersion curve during these frequency intervals, shown in Figure 2.1(c), characterizes the evanescent nature of waves at those Bragg bandgaps.

Propagating branches in band structures in Figure 2.1(d) exhibit periodicity in k space, which is often referred to as the reciprocal space. They depict waves folding at $k = \pi/L$, where L is the length of the unit cell. Subsequent enclosed regions of symmetry from real bands in k space are called *Brillouin zones,* accredited to Leon Brillouin [14]. A primitive cell in the k space is the first Brillouin zone, which would be utilized to show the results, which can then be periodically expanded to the entire k space.

$E1 = 6.9\text{x}10^4 \text{N}/m^2$ $E2 = 5.5\text{x}10^5$ N$/m^2$
$\rho 1 = 2.0\text{x}10^3\text{kg}/m^3$ $\rho 2 = 2.7\text{x}10^3\text{kg}/m^3$
$L1$ =0.1m $L2$ =0.1m
Lattice Parameter = $L1 + L1 = 0.2m$

(a) Unit cell details

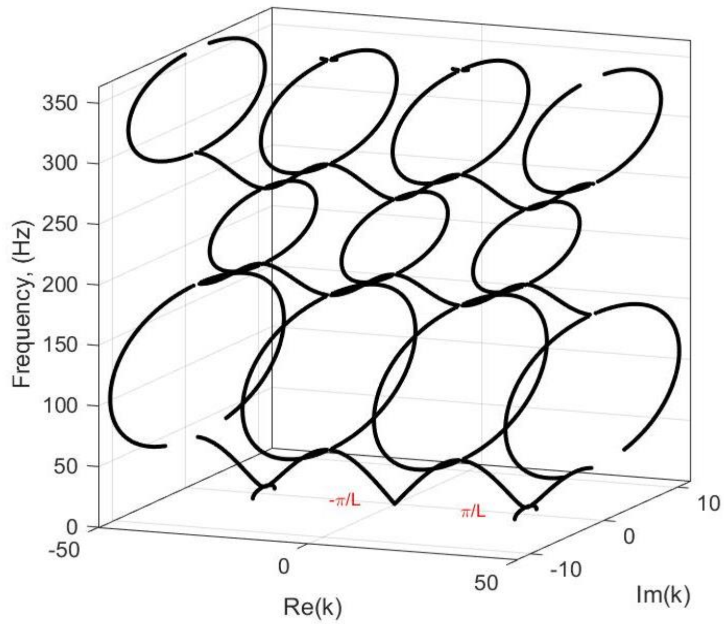

(b) Complex band structure

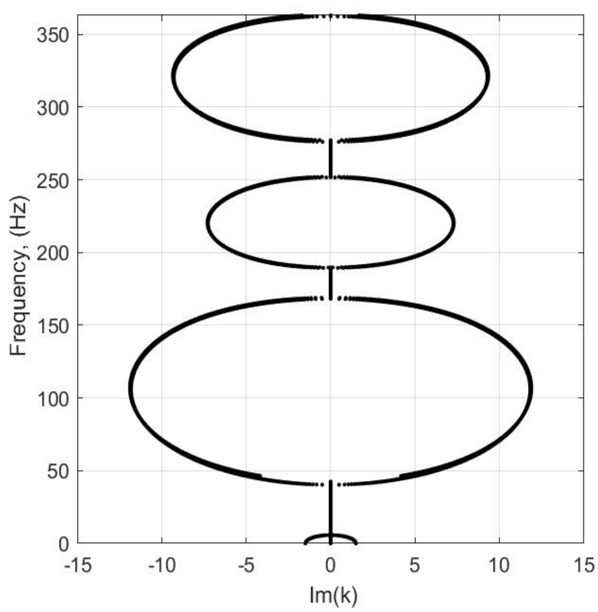

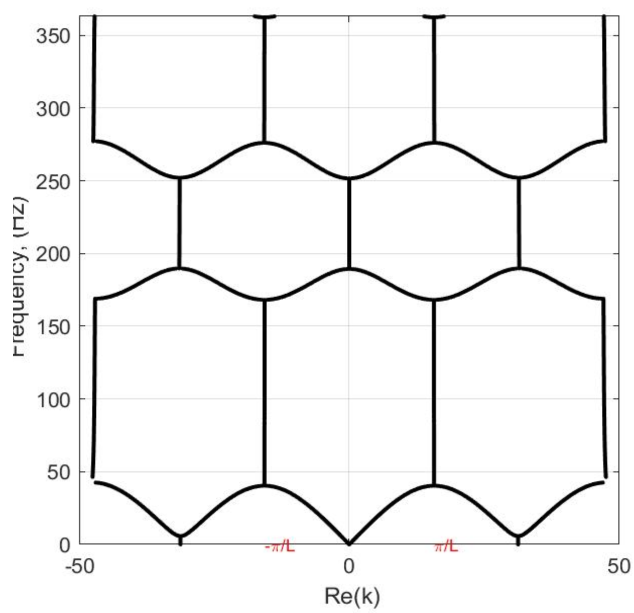

(c) Imaginary part of the band structure **(d) Real part of the band structure**

Figure 2.1: Model problem on 1D undamped phononic crystal and computed complex band structure using FEM based $\boldsymbol{k(\omega)}$ formulation

3 Padé Interpolation for Complex Band Structures

3.1 Padé Interpolation: Preliminaries

Let's assume $\kappa(\omega)$ is adequately smooth function of ω and $\{\omega_1, \omega_2, \omega_3, \omega_4, \ldots\ldots\ldots, \omega_L\}$ be L complex numbers, with corresponding wave numbers $\kappa(\omega_j)$ that are already computed. Padé approximants for κ, which can be used to compute wavenumber at other frequencies, is defined:

$$\kappa(\omega) \cong \frac{P_N(\omega)}{Q_M(\omega)} = \kappa_p(\omega), \tag{3.1}$$

where,

$$P_N(\omega) = \sum_{r=0}^{N} p_r \omega^r \ ; \ \ Q_M(\omega) = 1 + \sum_{r=1}^{M} q_r \omega^r.$$

Eq. (3.1) can be expanded into,

$$\kappa_{p\,j} = \frac{p_0 \ + p_1\ \omega_j + p_2\, \omega_j^2 + p_3\, \omega_j^3 + \ldots\ldots\ldots\ldots\ldots + p_N \omega_j^N}{1 \ + q_1\ \omega_j + q_2\, \omega_j^2 + q_3\, \omega_j^3 + \ldots\ldots\ldots\ldots\ \ + q_M \omega_j^M}\ \ , \tag{3.2}$$

for j= 1, 2, 3, ……. , L. And subsequently, $N + M + 1 = L$.

In our work, only diagonal rational function for κ_p will be considered, i.e.,

$M = N + 1$ If L is even,

and $M = N$ If L is odd.

Rewriting Eq. (3.2) in a linear form results in:

$$\kappa_{p\,j}\{1 + q_1\ \omega_j + q_2\, \omega_j^2 + \ldots\ldots + q_M \omega_j^M\} = \ p_0 + p_1\ \omega_j + p_2\, \omega_j^2 + \ldots\ldots + p_N \omega_j^N. \tag{3.3}$$

The above equation is repeated for j= 1, 2, 3, ... , L , resulting in,

$$\begin{bmatrix} 1 & \omega_1 & \omega_1^2 & \omega_1^3 & ..\omega_1^N & -\kappa_{p\,1}\omega_1^1 - & \kappa_{p\,1}\omega_1^2 .... & -\kappa_{p\,1}\omega_1^M \\ 1 & \omega_2 & \omega_2^2 & \omega_2^3 & ..\omega_2^N & -\kappa_{p\,2}\omega_2^1 - & \kappa_{p\,2}\omega_2^2 .... & -\kappa_{p\,2}\omega_2^M \\ . & . & . & . & . & . & . & . \\ . & . & . & . & . & . & . & . \\ . & . & . & . & . & . & . & . \\ 1 & \omega_L & \omega_L^2 & \omega_L^3 & ..\omega_L^N & -\kappa_{p\,L}\omega_L^1 - & \kappa_{p\,L}\omega_L^2 .... & -\kappa_{p\,L}\omega_L^M \end{bmatrix} \boldsymbol{x} = \boldsymbol{y} \tag{3.4}$$

where $\boldsymbol{x}$ and $\boldsymbol{y}$ are complex valued vectors representing the Padé parameters and function values at the interpolation points respectively:

$$\boldsymbol{x} = \{\ p_0 \ \ p_1 \ \ p_2 \ . \ . \ . \ . \ p_N \ \ q_1 \ \ q_2 \ . \ . \ . \ q_M\}^{\mathrm{T}}, \tag{3.5}$$

$$\boldsymbol{y} = \{\ \kappa_{p\,1} \ \ \kappa_{p\,2} \ \ \kappa_{p\,3} \ . \ . \ . \ \kappa_{p\,N} \ \ \kappa_{p\,N+1} \ \kappa_{p\,N+2} \ . \ . \ . \ \kappa_{p\,L}\}^{\mathrm{T}}.$$

Solving for the Padé parameters $\boldsymbol{x}$, and substituting them into Eq. (3.2) will result in the Padé interpolation function $\kappa_p(\omega)$ for the given interpolation points.

Often, to facilitate a better approximation, $\kappa_p(\omega)$ can be defined on overlapping sub-intervals $\mho_{\omega\,r} \subset [0 \ \ \omega_L]$ with corresponding interpolation functions $\kappa_p{}^{\mho_{\omega\,r}}(\omega)$. Each $\kappa_p^{\mho_{\omega\,r}}(\omega)$ will be determined using above framework (Eq. (3.2) to Eq. (3.5)) for different intervals of ω. This is referred to as *piecewise Padé interpolation*. Thus, $\kappa(\omega)$ can now be approximated as,

$$\kappa(\omega) \cong \kappa_p(\omega) = \begin{cases} \kappa_p{}^{\mho_{\omega\,1}} & \text{if} \quad \omega \in \mho_{\omega\,1} \\ \kappa_p{}^{\mho_{\omega\,2}} & \text{if} \quad \omega \in \mho_{\omega\,2} \\ & . \\ & . \\ \kappa_p{}^{\mho_{\omega\,r}} & \text{if} \quad \omega \in \mho_{\omega\,r} \\ & . \\ & . \\ \kappa_p{}^{\mho_{\omega\,z}} & \text{if} \quad \omega \in \mho_{\omega\,z} \end{cases}, \tag{3.6}$$

where, $\mho_{\omega\,r} \subset [0 \ \ \omega_L]$, for $r = 1 \ldots z$.

3.2 A Closer Look at Band Structure

3.2.1 Intervals of Interpolation: Resonant Frequencies

Complex band structure in the *irreducible Brillion zone* (IRBZ), i.e. *the symmetrical half of the first Brillouin zone*, for each direction of $\boldsymbol{k}$ can be thought of as a smooth mapping of $\omega \in R$ into a $\boldsymbol{k}$- ω complex plane. The $\boldsymbol{k}(\omega)$ formulation for any propagation direction $\theta = \theta_j$, can be shown as,

$$\kappa(\omega) \quad \Longleftarrow \left[(-\omega^2\boldsymbol{\mathcal{M}} + \boldsymbol{\mathcal{K}}) + i\kappa\boldsymbol{H}(\theta_j) - (i\kappa)^2\boldsymbol{A}(\theta_j)\right]_{\Omega_n} \boldsymbol{d} = \boldsymbol{0}. \tag{3.7}$$

With increasing frequency ω, complex bands in IRBZ alternate between propagating and evanescent branches, while bounded in real($\boldsymbol{k}$)-axis between zero and Bragg plane (the perpendicular bisector in k space that demarcates Brillouin zones).

Set of frequencies on complex band structure corresponding to $\boldsymbol{k} = 0$, are referred to as *resonant frequencies* (ω_{res}). These resonant frequencies mark the transition between propagating and evanescent regimes and will be used to automatically guide us in choosing the Pade interpolation intervals and the corresponding interpolation points. The resonant frequencies can be computed from Eq. (3.7), specialized for $\boldsymbol{k} = 0$, taking the simplified form,

$$[\,\omega_{res}{}^2\boldsymbol{\mathcal{M}} + \boldsymbol{\mathcal{K}}\,]\,\boldsymbol{d} = \boldsymbol{0}. \tag{3.8}$$

Since ω_{res} demarcate the propagation/evanescent transition, we can therefore define the *bounds* for individual segment intervals for piecewise Padé function in Eq. (3.6). *A resonant frequency* based, "$z - i$intervals" for piecewise Padé are as follows,

$$
\begin{aligned}
\mho_{\omega\,1} &= [\omega_{res\,1}\,, \dots\dots\dots, \omega_{res\,2}] \\
\mho_{\omega\,2} &= [\omega_{res\,2}\,, \dots\dots\dots, \omega_{res\,3}] \\
&\;\;\vdots \\
\mho_{\omega\,r} &= [\omega_{res\,r}\,\;, \dots\dots\dots, \omega_{res\,r+1}] \\
&\;\;\vdots \\
\mho_{\omega\,z} &= [\omega_{res\,z}\,, \dots\dots\dots, \omega_{res\,z+1}]
\end{aligned} \tag{3.9}
$$

where, $\mho_{\omega\,r}$ is a set of frequencies used for piecewise Padé interpolation on a complete segment of either a propagating branch or an evanescent mode.

3.2.2 Padé Interpolation Points

With reference to Figure. 2.1 (b), complex dispersion relations portray *circular bands* for either harmonic propagative branches or decaying evanescent modes. To capture the curvatures of the modes in generating *Padé interpolation points* for each interval $\mho_{\omega\,r}$, we adopted the *ad hoc* approach used for generalized continued fraction for absorbing boundary conditions in [15]. Specifically, the interpolation points are given by,

$$
\mho_{\omega\,r} = \frac{1}{2}\left(\omega_{res\,r} + \omega_{res\,r+1}\right) - \frac{1}{2}\left(\omega_{res\,r+1} - \omega_{res\,r}\right)\cos\alpha, \tag{3.10}
$$

$$
\alpha = \frac{\pi}{np}m \;\; ; \;\; 0 \leq \frac{\pi}{np}m \;\leq\; \pi, \;\; \text{m=1, 2….}
$$

In the above expressions, *np* is the number of interpolation points for a segment interval $\mho_{\omega\,r}$, which is a parameter of the proposed method.

3.2.3 Number of Padé Interpolation Points

Convergence of Padé interpolation scheme based on complex band structure for 1D phononic crystal was tested and compared to a Lagrange polynomial interpolation on a resonant region with sharp transition from propagation to non-propagation for the same number of interpolation points. Figures 3.1(a) and (b), demonstrate that, while polynomial interpolation leads to significant oscillations with large errors, Padé interpolation captures the complex band structure effectively, without any oscillations, and with much smaller error. A more quantitative convergence analysis is done to compare the two interpolation approaches in Figures 3.2 (a) and (b), where the relative error defined as,

$$\text{Relative Error} = \frac{|\,\kappa_{exact} - \kappa_h\,|}{\kappa_{exact}}, \tag{3.11}$$

is plotted with respect to the interpolation points using frequencies in the transition region. Clearly, the proposed Pade interpolation provides fast convergence leading to fewer interpolation points and less computational cost. It can further be seen that for satisfactory accuracy, np can be chosen between 4 and 8 per interval $\mho_{\omega\, r}$.

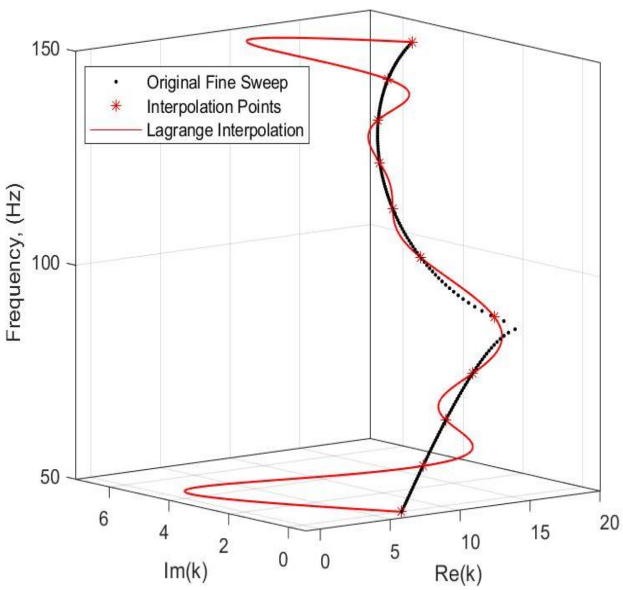

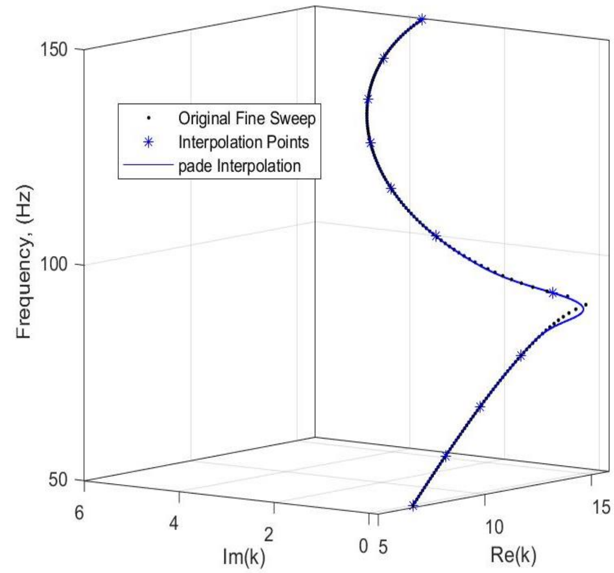

(a) Interpolation of complex band structure using Lagrange polynomial with 11 interpolation points.

(b) Interpolation of complex band structure using Padé interpolation combining two resonant frequency intervals $\mho_{\omega r}$, with np=5 and np=6

Figure 3.1: Stability comparison of Padé interpolation scheme and Lagrange interpolation

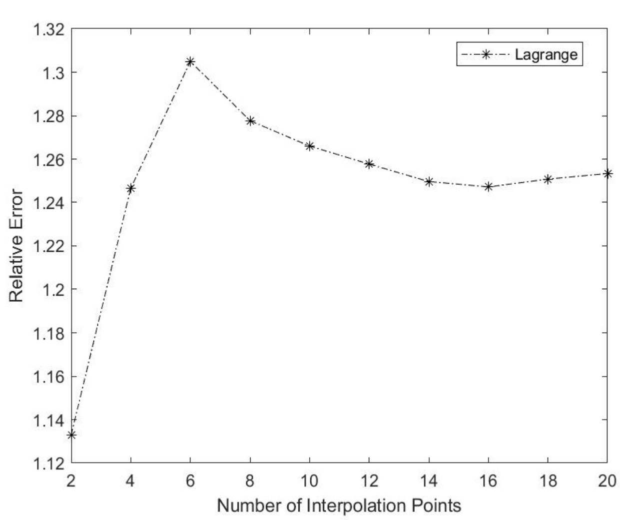

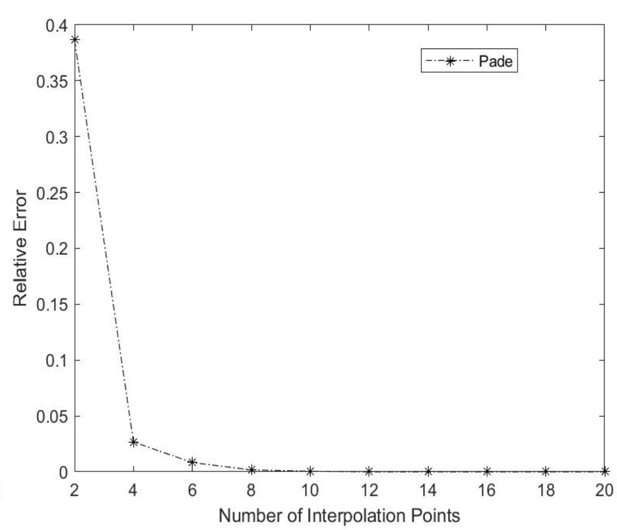

(a) Convergence study for Lagrange polynomial as a function of number of interpolation points

(b) Convergence study for Padé interpolation as a function of number of interpolation points

Figure 3.2: Convergence comparison of Padé interpolation scheme and Lagrange interpolation

3.2.4 Effectiveness of the Proposed Approach: Model Problem

A model problem in Section 2.3 of a 1D bi-material phononic crystal is revisited to show the effectiveness of the Padé interpolation scheme. Resonant frequencies ω_{res} are easily obtained through solving Eq. (3.8) using a composite unit cell obtained by combining two primitive unit cells. For higher dimensional phononic crystals, ω_{res} will be shown in Section 3.3.2 depending on the direction of propagation.

Frequency interpolation intervals $\mho_{\omega r}$ for piecewise Padé are set to overlap through resonant frequencies for a smooth interpolation of $\kappa(\omega) \cong \kappa_p(\omega)$ in Eq. (3.6). We alternate interpolation points, $np = 5$ for $\mho_{\omega r}$ in propagating regimes and $np = 6$ for $\mho_{\omega r}$ in evanescent regimes. The choice for minimum number of interpolation points for good approximation was based on the pilot convergence study in Figure 3.2(b).

The original complex band plot (green) in Figure 3.3 was initially computed through fine frequency sweeping at 0.3Hz-interval for a frequency band of [0-700] Hz using Eq. (2.12) This resulted in solving a polynomial eigenvalue problem 2334 times. A proposed reduced computation technique by Padé interpolation approach allowed to solve the polynomial eigenvalue problem only 66 times for a frequency band of [0 720] Hz (blue stars) in Figure 3.3

12-intervals piecewise Padé interpolation functions were built based on approximants from every interval $\mho_{\omega r}$. Overlapped smooth interpolations (blue line) in Figure 3.3 accurately approximated the complex band with 97 percent reduction cost.

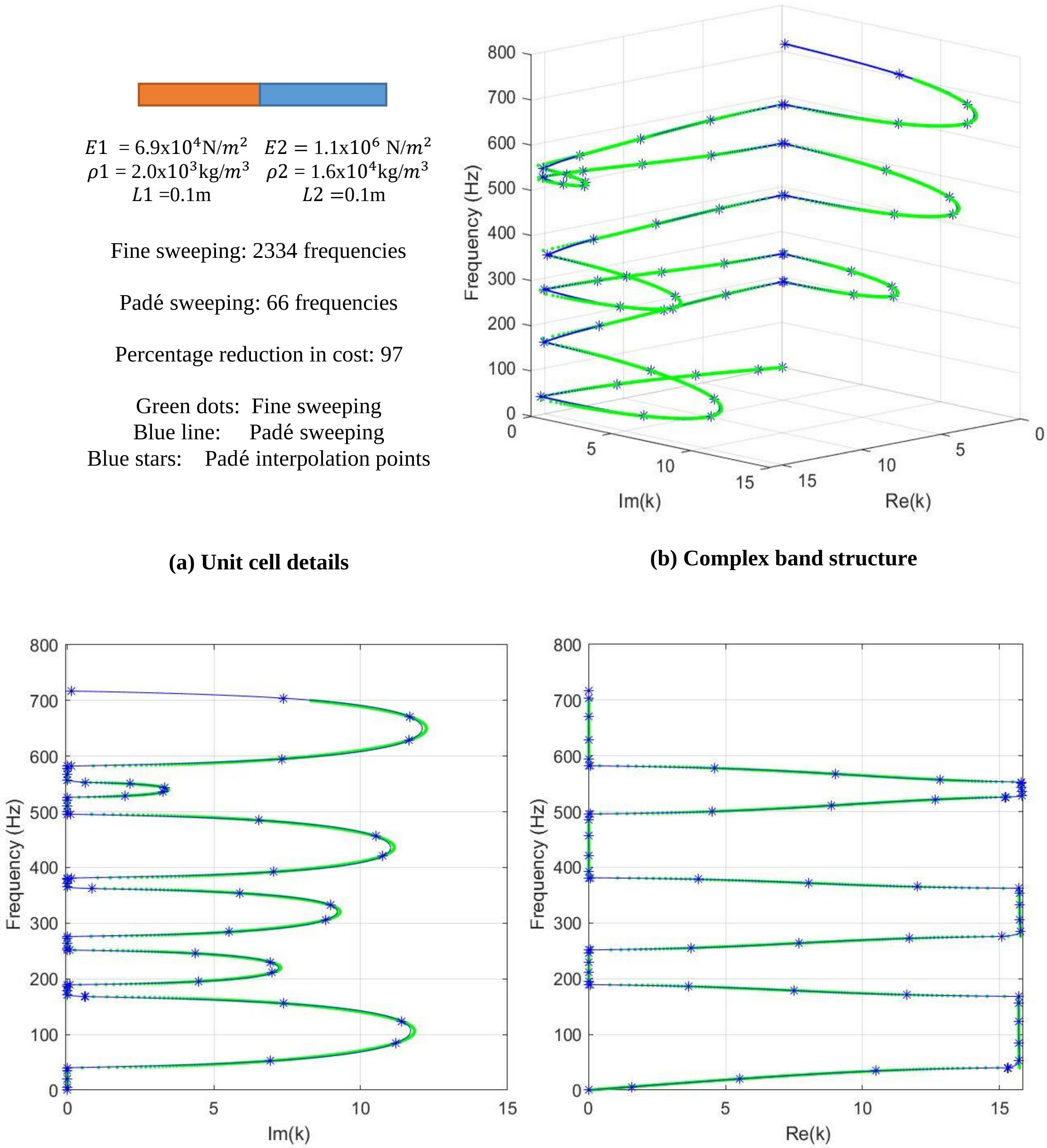

(a) Unit cell details

(b) Complex band structure

(c) Imaginary part of the band structure

(d) Real part of the band structure

Figure 3.3: Model problem on 1D undamped phononic crystal demonstrating efficacy of the proposed computation reduction scheme by Padé interpolation

3.3 Extension to Higher Dimensional Systems

3.3.1 Separating Multiple Branches using Modal Assurance Criterion

A variant of *Model Assurance Criterion* technique [16], which is a statistical indication to measure similarities and dissimilarities between vibrational mode shapes is utilized in identifying and isolating in-plane modes as *longitudinal modes* or *transverse modes* for 2D elastic and viscoelastic modeling. In our context, a pair of test vectors $\mathbf{v_{test}} = [\boldsymbol{v}_{\,long}\,(\omega_{test})\;\; \boldsymbol{v}_{\,trans}\,(\omega_{test})] \in \mathbb{C}^{n\,x\,2}$ on Ω_n inside the IRBZ associated with corresponding wavenumber vectors $\boldsymbol{k}_{long}\,(\omega_{test})$ and $\boldsymbol{k}_{trans}\,(\omega_{test})$ will be computed from any test frequency ω_{test} in either propagating regime or evanescent regime. An inner product of $\mathbf{v}_{\text{test}}$ was observed to yield,

$$0 < \langle \boldsymbol{v}_{\,long}\,(\omega_{test})\,, \mathbf{v_{test}}\,(\omega_{test})\,\rangle < 1, \tag{3.12}$$

where,

$$\left|\boldsymbol{v}_{\,long}\right| = |\boldsymbol{v}_{\,trans}| = 1.$$

A filtering indicator to separate modes was set based on Eq. (3.12) by taking advantage of orthogonality of modes into cross correlating every computed set of vectors from all frequencies of interest against $\mathbf{v_{test}}\,(\omega_{test})$, such that,

$$\langle \boldsymbol{v}_{\,long}\,(\omega_{test})\,, \mathbf{v}(\omega)\,\rangle = MAC \quad \forall\, \omega\, \in [0\;\; \omega_L]\,. \tag{3.13}$$

Whenever MAC is close to unity, the mode is considered longitudinal, while MAC close to zero indicates a transverse wave, thus facilitating the separation of the two modes. We note here that this preliminary approach is valid for simple unit cells, and a more elaborate approach is needed for general unit cells.

3.3.2 Resonant Frequencies for Higher Dimension

Resonant frequencies for 1D modeling can conveniently be obtained from using 2-unit cells by imposing periodic boundary conditions to solve for ω_{res} in Eq. (3.8). This, however, is an inefficient way to obtain resonant frequencies in higher dimensions. A generalized approach to compute ω_{res} from Eq. (3.8), is to separately enforce periodic boundary conditions and antiperiodic boundary conditions on one primitive unit cell, which are dependent on the propagation direction.

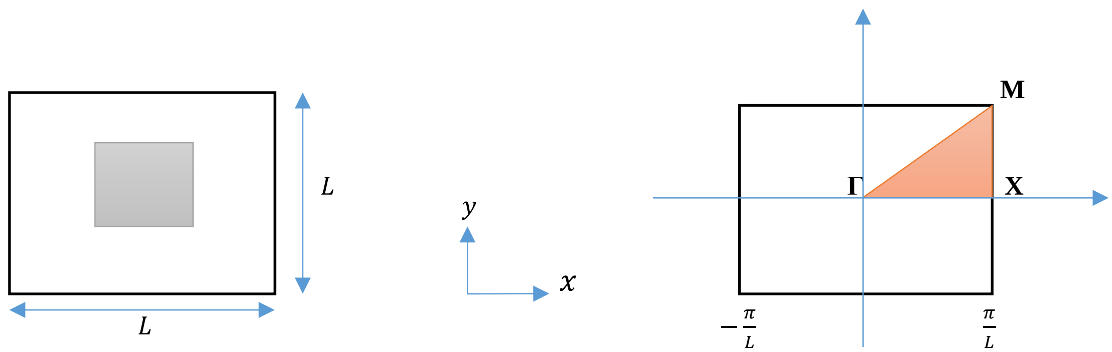

(a) Physical unit cell

(b) First Brillouin zone (IRBZ shaded)

Figure 3.4: A schematic of 2D phononic crystal unit cell (left) and the corresponding First Brillouin zone (right)

For simplicity, we explain resonance frequency computation for a square unit cell through the edges of IRBZ shown in Figure 3.4(b). Resonant frequencies can now be defined as transition frequencies, at $\boldsymbol{k} = 0$ and $\boldsymbol{k} =$ Bragg plane depending on propagation direction. Bloch-Floquet representation, Eq. (2.1) and Eq. (2.2) describing periodic solution $\tilde{\boldsymbol{u}}$, modulated by the phase $e^{i\boldsymbol{k}.\boldsymbol{x}}$, is used to determine boundary conditions for obtaining resonant frequencies from Eq. (3.8). This procedure is summarized in the self-explanatory Table 3.1.

Table 3.1: Boundary conditions in computing resonant frequencies along the edges of irreducible Brillouin zone for 2D phononic crystal

Γ		**X**		**M**	
$k_x = 0$	$k_y = 0$	$k_x = \frac{\pi}{L}$	$k_y = 0$	$k_x = \frac{\pi}{L}$	$k_y = \frac{\pi}{L}$
$e^{ik_xL} = 0$	$e^{ik_yL} = 0$	$e^{ik_xL} = -1$	$e^{ik_yL} = 0$	$e^{ik_xL} = -1$	$e^{ik_yL} = -1$
Periodic in x	Periodic in y	Antiperiodic in x	Periodic in y	Antiperiodic in x	Antiperiodic in y

3.4 Summary of the Algorithm

The algorithm developed in this study can be summarized using the following steps:

1. Compute critical frequencies with periodic and antiperiodic boundary conditions, as described in Section 3.3.2.
2. Separate the resonant frequencies into different modes based on modal assurance criterion, presented in Equation (3.13).
3. Determine the Padé intervals for each of the modes using the strategy presented in Section 3.2.1.
4. Determine the Padé interpolation points using Equation (3.10).
5. Compute complex wavenumbers for Padé interpolation frequencies by solving the quadratic eigenvalue problem in Equation (2.12).
6. Separate the wavenumbers into different modes using modal assurance criterion in Equation (3.13).
7. Perform Padé interpolation independently for each of the modes using Equation. (3.2) – Equation (3.6).

4. Numerical Examples

To illustrate the efficacy of Padé interpolation method in computing complex band structures, we consider both 1D and 2D phononic systems with different material configurations. 1D bi-material phononic crystals with viscous damping and 1D phononic metamaterials with spring-mass system as internal resonator were first investigated. Moreover, 2D undamped and viscously damped phononic crystals were also modelled to compute complex band structures through fine frequency sweeping using Eq. (2.12). Padé interpolation scheme proposed in this paper is then used to recompute complex bands for reduced number of frequencies, resulting in accurate results at a fraction of the computational cost.

4.1 1D Viscoelastic Phononic Crystals

A model problem on Section 3.2.4 for undamped 1D phononic crystal demonstrated the effectiveness of Padé interpolation in approximating complex bands. We further wanted to test the ability of the proposed scheme in capturing complex bands for viscously damped phononic crystals. Realization of 1D phononic crystal as continuous bars for complex bands with small damping and large damping are shown in Figures 4.1(a) and 4.2(a), respectively. The complex band structures were initially computed by fine frequency sweeping, 2334 times using Eq. (2.12). Resonant frequencies to define Padé intervals were computed from an undamped model (by ignoring viscosity) using two-unit cells. Padé interpolation points for each interval were chosen such that, $np = 5$. Interpolation frequencies (blue stars) in Figure 4.1 and Figure 4.2 resulted in a total of 66 sparse data points which translates to 97 percent reduction in computational cost.

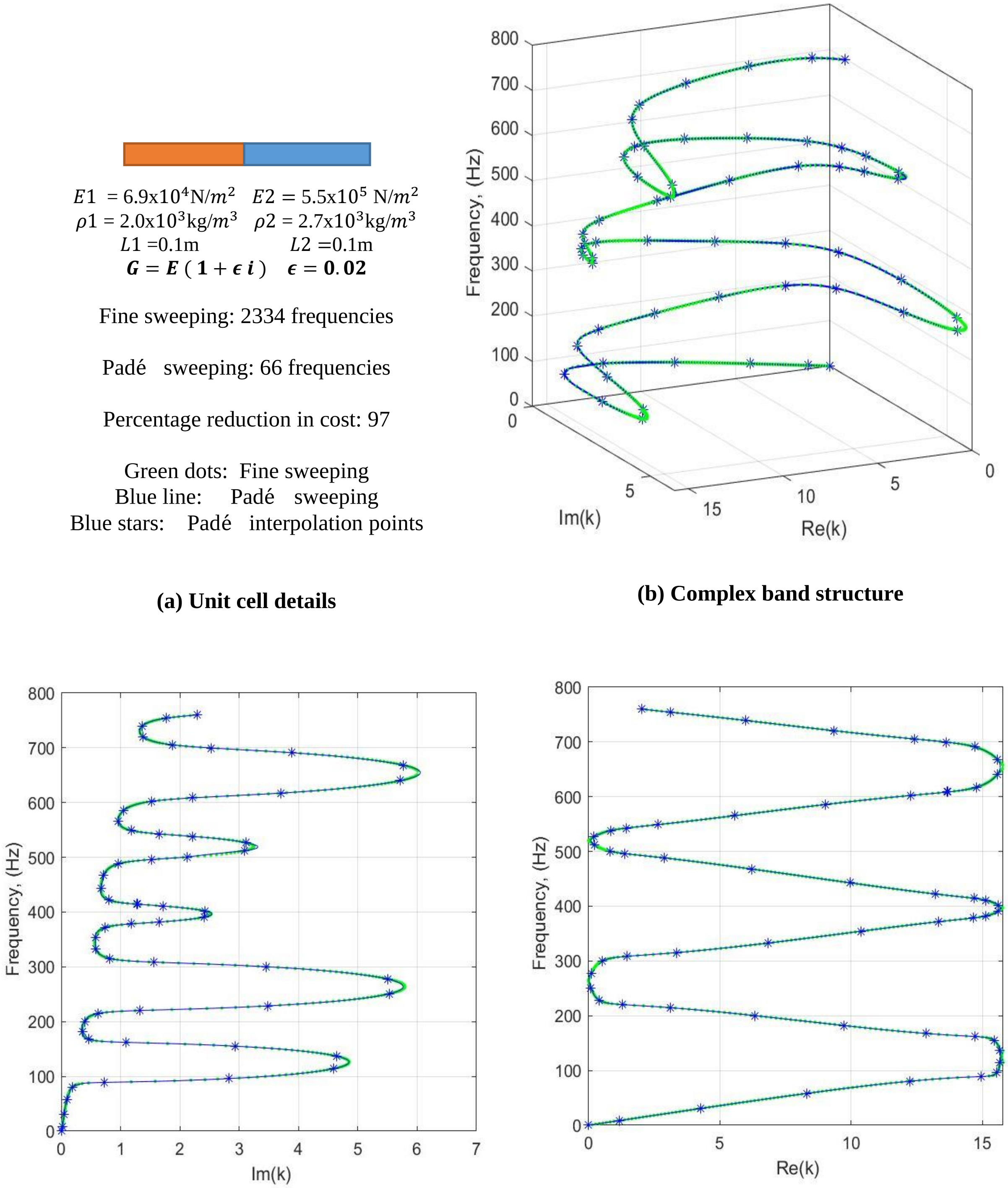

(a) Unit cell details

(b) Complex band structure

(c) Imaginary part of the band structure

(d) Real part of the band structure

Figure 4.1: 1D phononic crystal with small viscous damping and computed complex band structure through Padé interpolation scheme (blue plot)

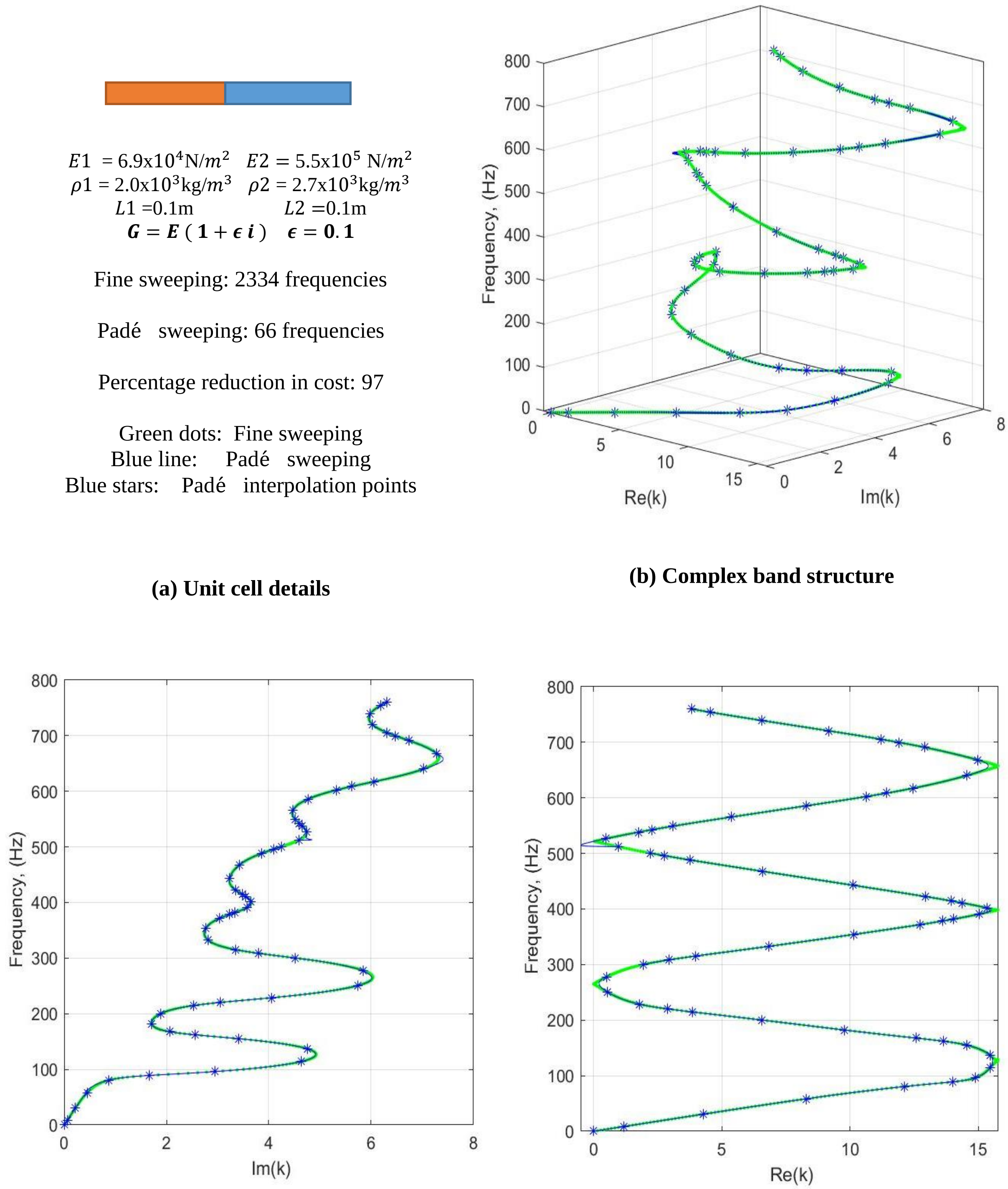

(a) Unit cell details

(b) Complex band structure

(c) Imaginary part of the band structure

(d) Real part of the band structure

Figure 4.2: 1D phononic crystal with large viscous damping and computed complex band structure through Padé interpolation scheme (blue plot)

4.2 1D Metamaterials

In this subsection, we explore separately a family of metamaterials for elastic Bloch waves. The first one is a bi-material bar with (non-viscous) spring mass system. Initial computational of complex bands for this model through fine frequency sweeping predicted a subwavelength bandgap due to the internal resonator which was centered at $= \sqrt{Ks/Ms}$, where Ks and Ms denote the spring stiffness and the attached mass respectively. The results are shown in Figure 4.3(b) (green dots). The second structure is a bi-material bar with viscous-spring mass system; this more complicated metamaterial exhibited a damped mode around the subwavelength material bandgap Figure. 4.4(b).

Computation of the complex band structure with fine frequency interval of 0.4 Hz resulted in the need to solve quadratic eigenvalue problem in Eq. (2.12), 901 times. Resonant frequencies were computed using both periodic and antiperiodic boundary conditions. Number of interpolation points for a (non-viscous) spring model was uniformly chosen for $np = 5$, for all interpolation intervals $\mho_{\omega\, r}$. For viscous-spring model, number of interpolation points were chosen slightly differently, with $np = 5$ in propagating regimes and $np = 6$ in evanescent regimes. The additional interpolation points for the evanescent regime was chosen to enrich the convergence in capturing complex band from a pilot study Figure 3.2(b). Interpolation points for (non-viscous) spring model (shown in Figure 4.3, blue stars), and for the viscous-spring model (shown in Figure 4.4, blue stars) lead to a total of 25 and 28 points respectively, which resulted in more than 95 percent reduction in the computational cost. Despite coarse frequency grid, Padé interpolation (blue line) from Figure 4.3 and Figure 4.4 yielded excellent accuracy.

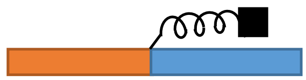

$E1 = 6.9\text{x}10^4 \text{N}/m^2$ $E2 = 5.5\text{x}10^5 \text{ N}/m^2$
$\rho 1 = 2.0\text{x}10^3 \text{kg}/m^3$ $\rho 2 = 2.7\text{x}10^3 \text{kg}/m^3$
$L1 = 0.1\text{m}$ $L2 = 0.1\text{m}$

Spring Stiffness $(Ks) = 7000\ N/m$
Mass attached to Spring $(Ms) = 1.5Kg$

Fine sweeping: 901 frequencies

Padé sweeping: 25 frequencies

Percentage reduction in cost: 97

Green dots: Fine sweeping
Blue line: Padé sweeping
Blue stars: Padé interpolation points

(a) Unit cell details

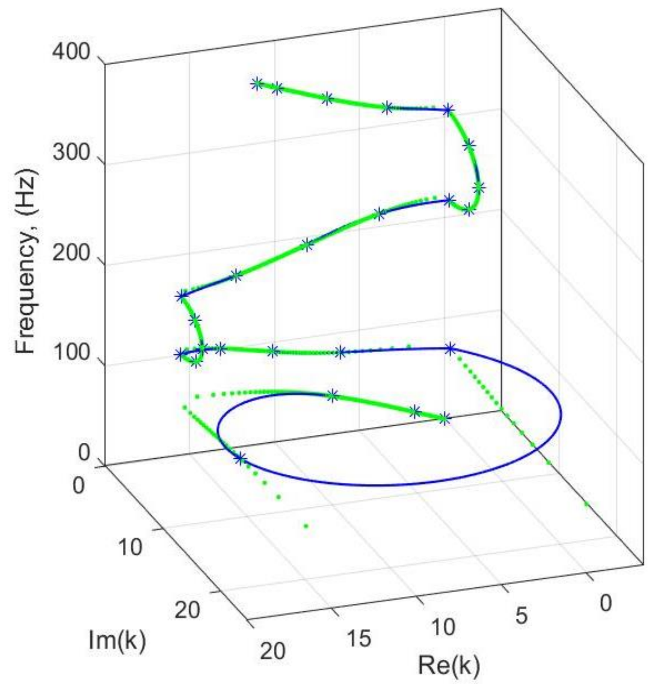

(b) Complex band structure

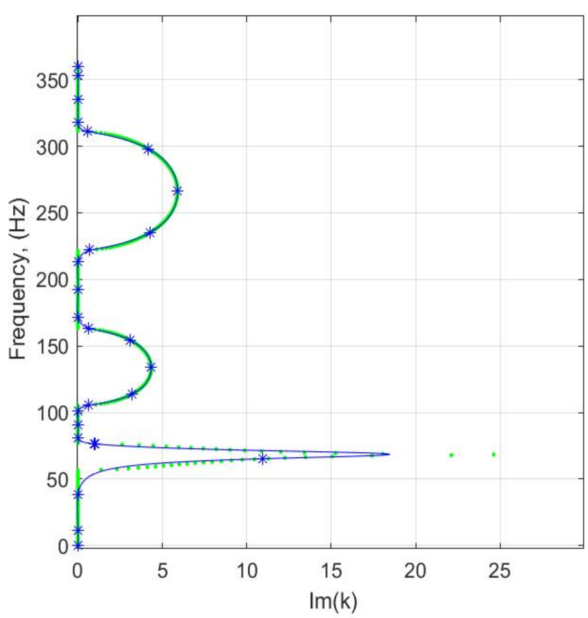

(c) Imaginary part of the band structure

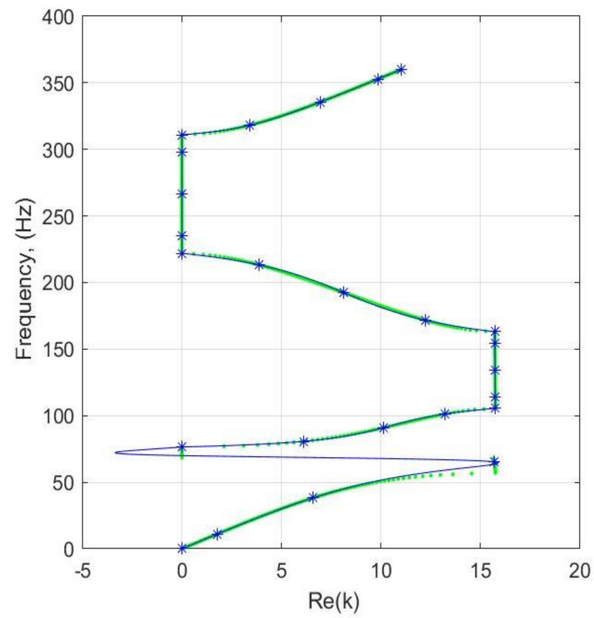

(d) Real part of the band structure

Figure 4.3: 1D metamaterial with spring mass system as internal resonator and computed complex band structures through Padé interpolation. The green curve is the result from fine frequency sweep, while the blue curve is the Padé-interpolation based computation. The blue stars represent the Padé interpolation points.

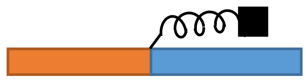

$E1 = 6.9\text{x}10^4 \text{N}/m^2$ $\quad E2 = 5.5\text{x}10^5 \text{ N}/m^2$
$\rho1 = 2.0\text{x}10^3 \text{kg}/m^3$ $\quad \rho2 = 2.7\text{x}10^3 \text{kg}/m^3$
$L1 = 0.1\text{m}$ $\quad L2 = 0.1\text{m}$

$Ks = (7000 + 1000\, i)\ N/m$
$Ms = 1.5Kg$

Fine sweeping: 901 frequencies

Padé sweeping: 28 frequencies

Percentage reduction in cost: 97

Green dots: Fine sweeping
Blue line: Padé sweeping
Blue stars: Padé interpolation points

(a) Unit cell details

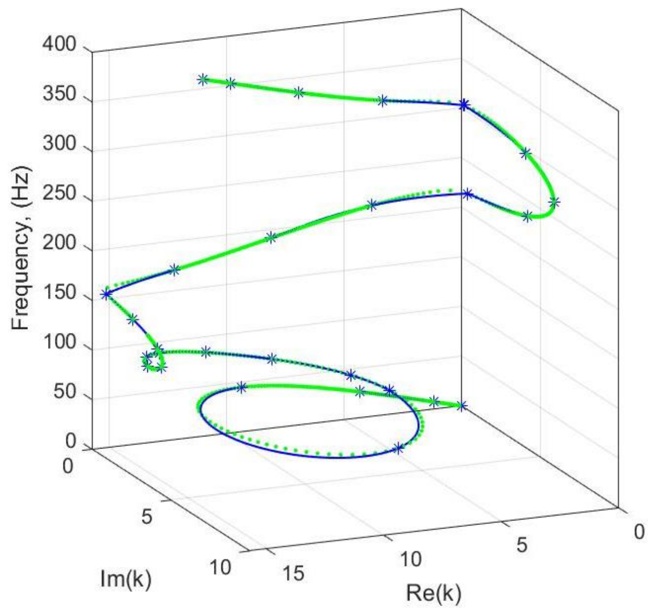

(b) Complex band structure

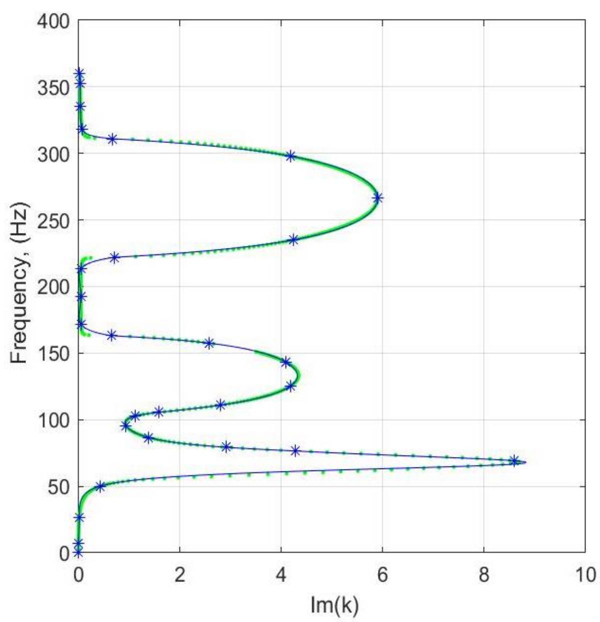

(c) Imaginary part of the band structure

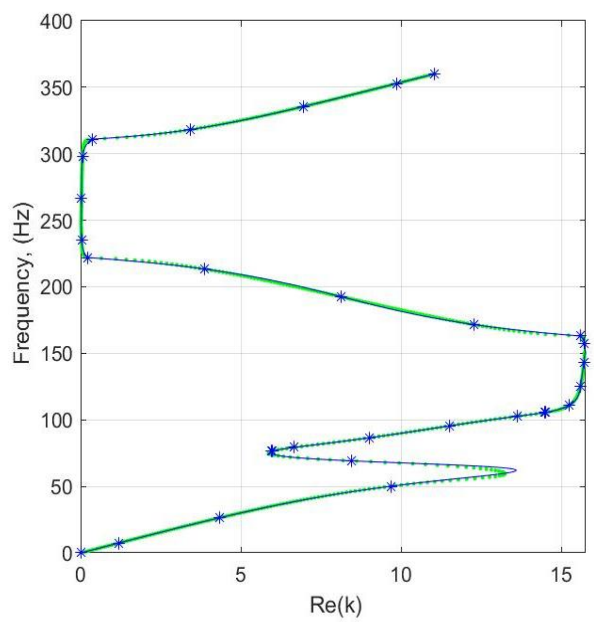

(d) Real part of the band structure

Figure 4.4: 1D metamaterial with viscous-spring mass system as internal resonator and computed complex band structures through Padé interpolation. The green curve is the result from fine frequency sweep, while the blue curve is the Padé -interpolation based computation. The blue stars represent the Padé interpolation points.

4.3 2D phononic crystals

Higher dimensional phononic systems exhibit both transverse and longitudinal modes. This is seen in both undamped and damped systems, as shown in Figures 4.6(a) and 4.7(a). They show the complex band structures for 2D damped and undamped bi-material phononic crystals under plane strain conditions, with horizontal wave propagation, i.e. $\theta = 0$. Computations of these complex band structures employed a discretized unit cell. As shown in Figure 4.5(c), the unit cell is meshed into 24x24 uniformly sized bilinear rectangular finite elements. Wave numbers, i.e. eigenvalues from Eq. (2.12), are computed on a fine frequency grid.

As discussed on Section 3.4, the modal assurance criterion for mode separation is integrated with the proposed Padé interpolation scheme (see Section 3.4). To determine Pade intervals, resonant frequencies were computed from linear eigenvalue problem using Eq. (3.8), with both periodic and antiperiodic boundary conditions as listed in Table 3.1. Resonant frequencies were then separated into individual longitudinal and transverse modes, again based on modal assurance criterion. Padé interpolation intervals for both longitudinal and shear modes can be used separately to obtain interpolation points for each mode individually. For better computational efficiency, however, we adopted a modified approach of using longitudinal mode interpolation intervals with uniform interpolation points, $np = 8$ for every interval $\mho_{\omega r}$. Total interpolation points resulted into 40 frequencies (blue stars or red stars) in Figure 4.6 and Figure 4.7, as opposed to a total of 361 frequencies (green dots) in same figures from initial fine sweeping (this translates to approximately 88% cost savings).

Padé interpolation was then performed for each mode individually (blue line and red line) for both structures, and are presented in Figures 4.6 and Figure 4.7, which clearly illustrates the accuracy of the proposed approach.

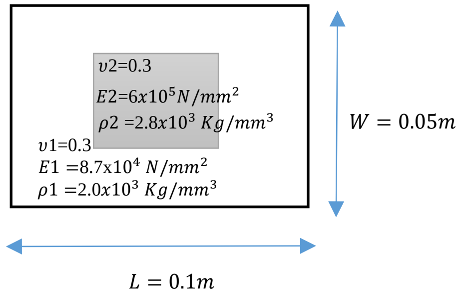

(a) 2D, bi-material, Wigner-Seitz cell

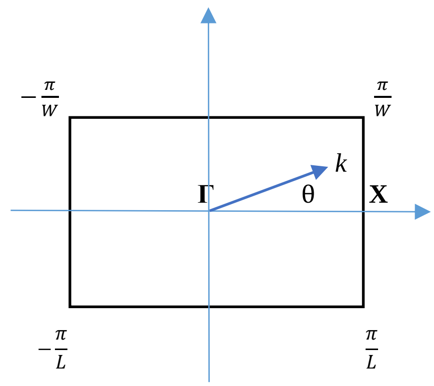

(b) First Brillouin Zone

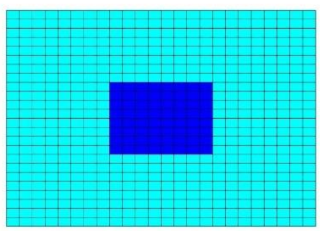

(c) FEM refined mesh

Figure 4.5: 2D phononic crystal: (a) physical cell material characteristics, (b) First Brillouin zone, (c) discretized mesh

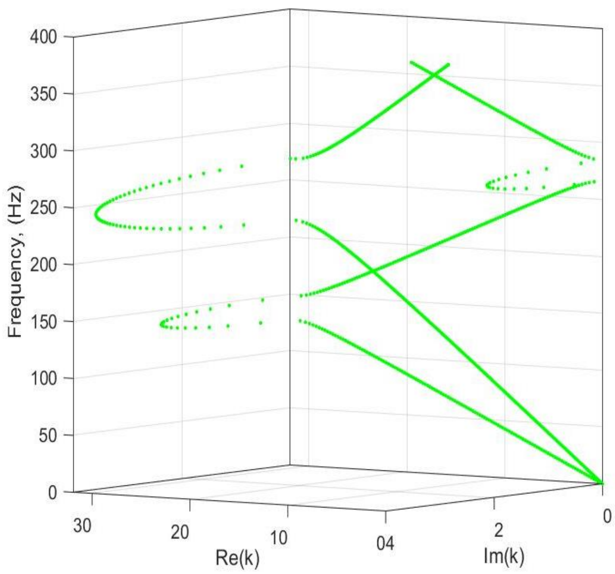

(a) Complex band structure through fine frequency sweeping

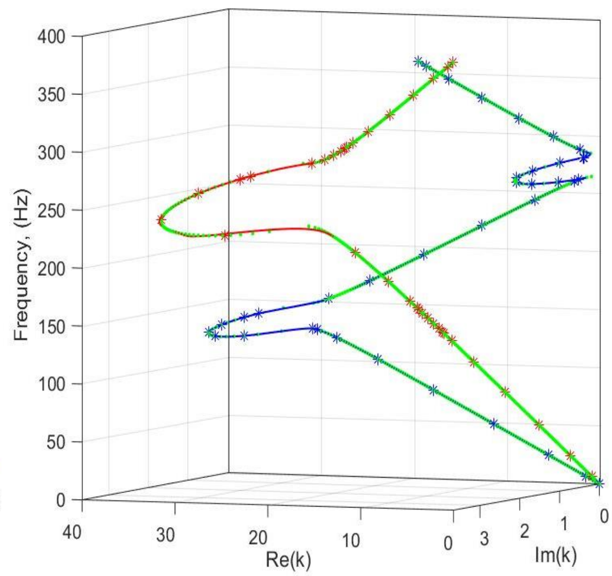

(b) Complex band structure

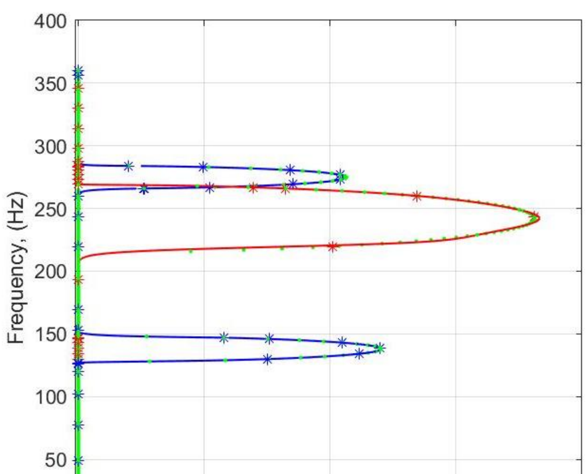

(c) Imaginary part of the band structure

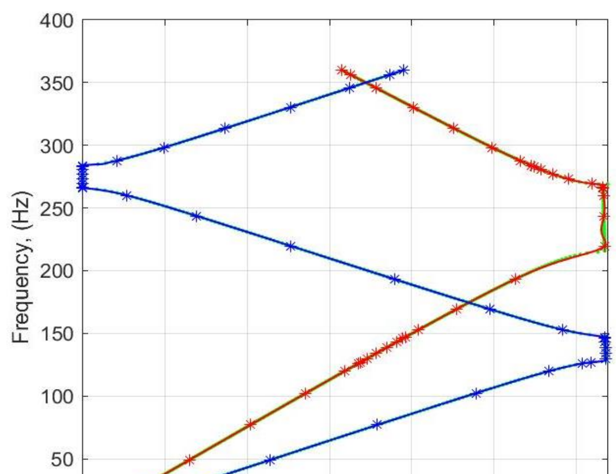

(d) Real part of the band structure

Figure 4.6: Complex band structure for 2D undamped phononic crystal with longitudinal (red) and transverse (blue) modes

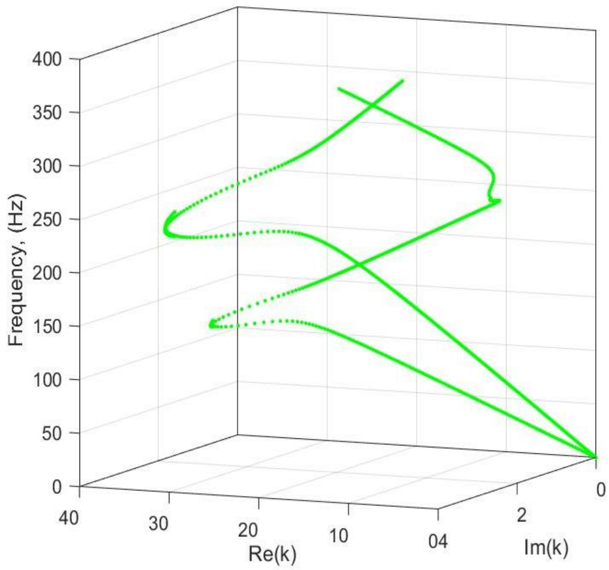

(a) Complex band structure through fine frequency sweeping

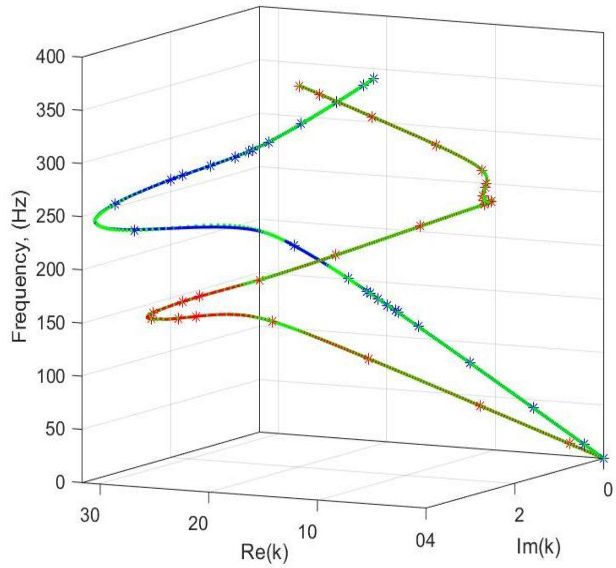

(b) Complex band structure

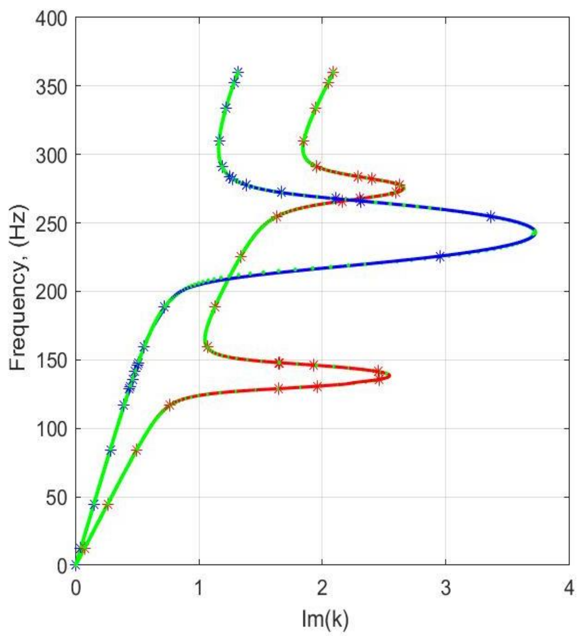

(c) Imaginary part of the band structure

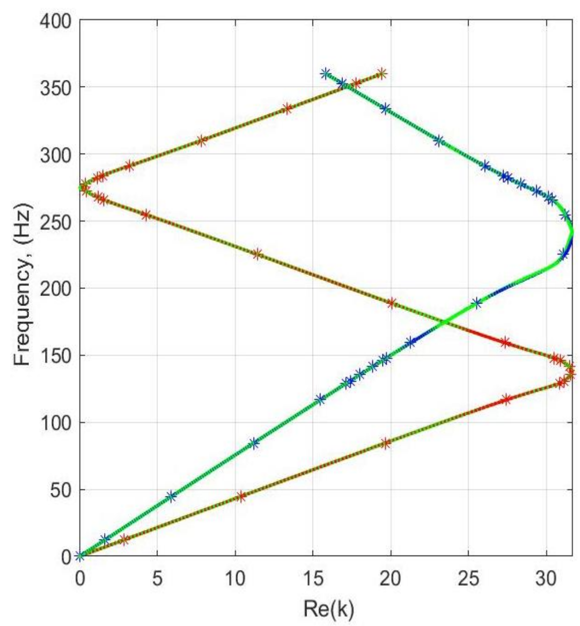

(d) Real part of the band structure

Figure 4.7: Complex band structure for 2D damped phononic crystal with longitudinal (red) and transverse (blue) modes

5. Concluding Remarks

We propose a technique to reduce the computational effort for calculating complex band structures of phononic crystals and metamaterials through Padé interpolation. The salient features of the method are to (a) divide the frequency range into multiple intervals with the help of (approximate) resonant frequencies associated with center and edge of the Brillouin zone, and (b) applying Padé interpolation in each interval to compute the full complex-band structure, with the computation of complex wavenumbers for just a handful of frequencies. This results in an order-of-magnitude reduction in the computational cost. A wide range of examples are shown in this paper, including 1D and 2D phononic crystals and metamaterials, which illustrate the effectiveness of Padé interpolation.

The current work is however preliminary in nature; future studies could be aimed at, (a) further *a priori* optimization of Padé intervals and interpolation points, (b) extension of the approach to oblique propagation angles, (c) combining the proposed approach with modal reduction techniques to further reduce the computation cost. With these refinements, the proposed approach would lead to practical computation of complex band structures of complicated 3D unit cells.

REFERENCES

[1] Sigalas, M. M., and Economou, E. N., 1992, “Elastic and Acoustic Wave Band Structure”, Journal of Sound and Vibration, **158**(2), pp. 377-382.

[2] Liu, Z. Y., Zhang, X. X., Mao, Y. W., Zhu, Y .Y., Yang, Z. Y., Chang, Chan, C. T., and Sheng, P., 2000, “Locally Resonant Sonic Materials”, Science, **289**(5485), pp. 1734-1736.

[3] Bragg, W. H., and Bragg, W. L., 1913, “The Reflection of X-rays by Crystals”, Proceedings of the Royal Society A: Mathematical, Physical and Engineering Sciences, **88**(605), pp. 428-438.

[4] Krushynska, A. O., Miniaci, M., Bosia, F., and Pugno, N. M., 2016, “Coupling Local Resonance with Bragg Band Gaps in Single-Phase Mechanical Metamaterials”, Extreme Mechanics Letters, **12**(2017), pp. 30-36.

[5] Hussein, M. I., Leamy, M. J., Ruzzene, M., 2014, “Dynamics of Phononic Materials and **66**(4), Structures: Historical Origins, Recent Progress and Future Outlook”, Applied Mechanics Reviews, p. 040802.

[6] Bavencoffe, M., Morvan, B., Izbicki, J. L., and Hladky, A. C., 2009, “Characterization of Evanescent Ultrasonic Waves in a Band Gap of a 1D Phononic Crystal”, IEEE International Ultrasonics Symposium, pp. 1024-1027.

[7] Laude, V., Achaoui, Y., Benchabane, S., and Khelif, A., 2009, “Evanescent Bloch Waves and Complex Band Structure of Phononic Crystals”, Physical Review B, **80**(9), p. 092301

[8] Veres, I. A., Berer, T., and Matsuda, O., 2013, “Complex Band Structures of Two Dimensional Phononic Crystals: Analysis by the Finite Element Method”, Journal of Applied Physics, **114**(8), p. 083519.

[9] Krushynska, A. A., and Meleshko, V. V., 2011, "Normal Waves in Elastic Bars of Rectangular Cross Section", The Journal of the Acoustical Society of America, **129**(3), pp. 1324-1335.

[10] Collet, M., Ouisse, M., Ruzzene, M., Ichchou, M. N., 2011, "Floque-Bloch Decomposition for Computation of Dispersion of Two-Dimensional Periodic, Damped Mechanical Systems", International Journal of Solids and Structures, **48**(20), pp. 2837-2848.

[11] Palermo, A., and Marzani, A., 2016, "Extended Bloch Mode Synthesis: Ultrafast Method for the Computation of Complex Band Structures in Phononic Media", International Journal of Solids and Structures, **100**, pp. 29-40.

[12] Hetmaniuk, U., Tezaur, R., and Farhat, C., 2012, "Review and Assessment of Interpolatory Model Order Reduction Methods for Frequency Response Structural Dynamics and Acoustics Problems", International Journal for Numerical Methods in Engineering, **90**(13), pp. 1636-1662.

[13] Bloch, F., 1929, "Über die Quantenmechanik der Elektronen in Kristallgittern", Zeitschrift für Physik, **52**, pp. 555–600.

[14] Brillouin, L., 1953, "Wave Propagation in Periodic Structures: Electric Filters and Crystal Lattices", Dover Publications.

[15] Guddati, M. N., and Tassoulas, J.L., 2000, "Continued-Fraction Absorbing Boundary Conditions for Wave Equation", Journal of Computational Acoustics **8**(01), pp. 139-156.

[16] Allemang, R. J., 2003, "The Model Assurance Creterion-Twenty Years of Use and Abuse", Sound and Vibration, **37**(8), pp. 14-21.